Journal of Materials Chemistry A

ROYAL SOCIETY OF CHEMISTRY

PAPER

View Article Online
View Journal | View Issue

Cite this: J. Mater. Chem. A, 2022, 10, 16182

How to switch from a poor PEDOT:X oxygen evolution reaction (OER) to a good one. A study on dual redox reversible PEDOT:metallacarborane†

Jewel Ann Maria Xavier, ‡[a] Isabel Fuentes, ‡[a] Miquel Nuez-Martínez,[a] Zsolt Kelemen,[a] Andreu Andrio,[b] Clara Viñas,[a] Vicente Compañ[c] and Francesc Teixidor *[a]

Received 16th March 2022
Accepted 27th June 2022

DOI: 10.1039/d2ta02079c

rsc.li/materials-a

Over the years, extensive research has been carried out to optimize the oxygen evolution reaction (OER) by adopting different techniques as well as catalysts. Conducting organic polymers such as PEDOT have been employed to study the reaction but have failed to lower the over-potential for the reaction. Here we show electrochemically made, intimately blended, dual redox reversible materials incorporating PEDOT and metallacarboranes. The metallacarboranes act as doping agents but with tunable $E_{1/2}$ potentials. The tunability of $E_{1/2}$ allows the overlapping of the two redox potentials which subsequently leads to their synergy. The physico-chemical properties of the metallacarboranes fade and become integrated with PEDOT to form a dual redox reversible system. Therefore, the properties of the dopant are modified by the polymer. Thus, due to its high $E_{1/2}$, the $Co^{4+/3+}$ couple would not be an efficient electrocatalyst for water oxidation but when it is immersed in the PEDOT matrix the $Co^{4+/3+}$ potential is more accessible so that very low overpotential values are obtained, which justifies the title of the work, *How to switch from a poor PEDOT:X oxygen evolution reaction (OER) to a good one*. The dual redox reversible system has been extensively characterized and has been shown to be a promising candidate for the water oxidation reaction.

Introduction

Conducting organic polymers (COPs) act as a bridge between metal and semiconductor electrical conductivity. Generally, the electrical properties of COPs can be tuned by using modified monomers such as thiophene which leads to polythiophene (PT) and its derivatives, 3,4-ethylenedioxythiophene which leads to poly(3,4-ethylenedioxythiophene) (PEDOT).[1] In order for these polymers to be conductive, they need to be partially oxidized. By being oxidized, a number of positive charges are generated on the backbone of the polymer, which require counter-anions or doping agents to achieve charge neutrality. The most commonly employed and commercially available COP is PEDOT:PSS where polystyrene sulfonate acts as the doping anion. PEDOT:PSS polymers are employed as thermoelectric materials having high efficiency,[2] as the electrolyte in polymer electrolytic capacitors,[3] as flexible organic cells,[4] as light emitting diodes[5] and as an alternative to indium tin oxide.[6] In contrast, redox polymers are those which alter their electrochemical properties with a change in the oxidation state in a reversible manner. This is indeed a herculean task as the lack of availability of robust aqueous soluble doping anions, which are reversibly redox-active and are firmly bound to the polymer backbone without being covalently bonded, makes it hard to achieve such a system.

A prominent soluble doping agent would be polyoxometallates (POMs) which are soluble in water as well as organic solvents and can be derivatized to a certain degree.[7,8] A plethora of literature is available on the application and potential advantages of POMs,[9–13] yet very little literature exists on achieving a covalent linkage between the POM and the polymer while retaining all the desired properties of the POM.[12–20] In contrast, studies involving metallacarboranes as doping agents are scarce.[21–30] Even though they share many physical properties with POMs such as low charge density with a negative charge on the periphery[24,25] (POMs on oxygen atoms and metallacarboranes on hydrogen atoms), solubility,[26] both being anionic species with dimensions larger than the nanoscale and their couples displaying reversible redox behaviour,[27] they differ in that the metallacarboranes exhibit 3D aromaticity.[29]

[a]Institut de Ciència de Materials de Barcelona, ICMAB-CSIC, Campus Universitat Autònoma de Barcelona, Barcelona, 08193, Spain. E-mail: teixidor@icmab.es

[b]Departamento de Física Aplicada, Universidad Jaume I, Avda. Sos Baynat s/n, Castellón de la Plana, 12071, Spain

[c]Escuela Técnica Superior de Ingenieros Industriales, Departamento de Termodinámica Aplicada, Universitat Politècnica de València, Camino de vera s/n, Valencia, 46022, Spain

† Electronic supplementary information (ESI) available. See https://doi.org/10.1039/d2ta02079c

‡ These authors contributed equally to the work.

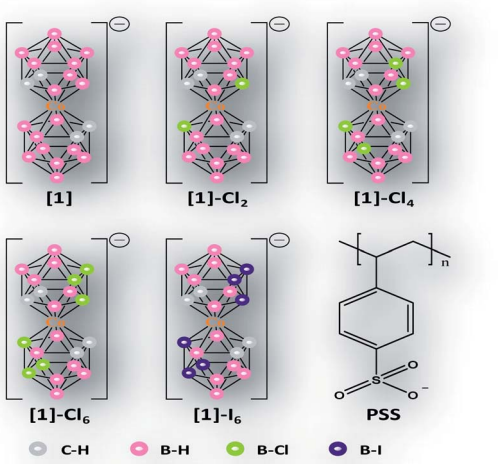

Scheme 1 Schematic representation of [1] and the halo-derivatives of [1] along with the reference anion employed in the study.

In this paper, we attempt a step forward in COPs and redox polymers by producing COPs that permit a voluntary fine tuning of their properties by modifying the redox potential of the doping agent to form a new COP having synergistic redox properties. These COPs have an added advantage of having two redox reversible components: the polymer backbone as well as the doping agent. Here, we show the potential application of metallacarboranes, a η^5 coordinated transition metal sandwich ligand,[28] as doping agents.

In this work, we have focused on $[Co(C_2B_9H_{11})_2]^-$, [1], and its halo-derivatives, [1]-Cl_x (x = 2, 4 and 6) and [1]-I_6 (Scheme 1), which can interact with the heteroatoms in PEDOT owing to its ability to form H-bonds and the presence of outer electron transfer elements. The paper also focuses on producing these dual redox reversible COPs in an electrochemical manner due to the high precision in terms of polymer composition.[30,31] The electrical properties of these dual redox reversible COPs have been extensively studied and discussed. Owing to the fact that PEDOT:PSS has been previously reported as a poor catalyst for oxidation reactions,[32] we have focused on demonstrating a potential application for the newly synthesized COPs as electrocatalysts in water oxidation.

Results

Electrochemical polymerization of PEDOT:[1]-X (X = Cl_x, x = 2, 4 and 6; I_6) and PEDOT:PSS

The compounds investigated in this study are: [1]-Cl_2, [1]-Cl_4, [1]-Cl_6 and [1]-I_6. The redox potentials for the pair $Co^{3+/2+}$ of [1], [1]-Cl_2, [1]-Cl_4, [1]-Cl_6 and [1]-I_6 are −1.28, −1.04, −0.85, −0.81 and −0.46 V *vs.* Ag/AgCl in dry acetonitrile, respectively (Fig. S1†).

Fig. 1 shows the different voltammograms recorded during the potentiodynamic synthesis of the samples in anhydrous acetonitrile. From the first cycle of the redox process, it can be observed that the $Co^{3+/2+}$ reduction occurs at −0.94, −0.80, −0.71 and −0.44 V *vs.* Ag/AgCl for PEDOT:[1]-Cl_x (x = 2, 4 and 6) and PEDOT:[1]-I_6, respectively. Therefore, the two different redox processes that can be observed from the voltammograms are the redox process of $Co^{3+/2+}$ and the redox process due to polymer formation. The redox processes due to PEDOT formation are quasi-identical for [1]-Cl_2 and [1]-Cl_4 considering the potential range and shape despite having different $E_{1/2}$ values for the redox process of $Co^{3+/2+}$. Conversely, the shape, potential range and the intensity for the redox process for PEDOT formation changes dramatically for [1]-Cl_6 with the intensity being 3–4 times higher than the other chloro-derivatives. In the case of [1]-I_6, the shape of the curve due to PEDOT formation is entirely different from the chloro-derivatives. The intensity of the CV is similar to [1]-Cl_2 but the capacitive current process is thinner in comparison.

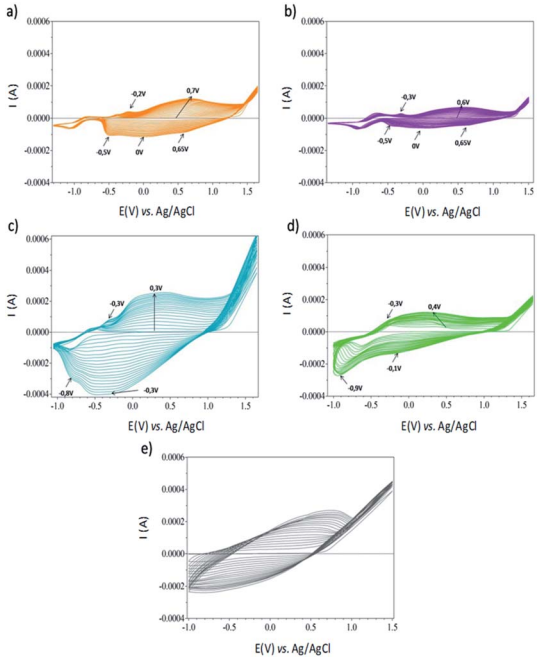

Fig. 1 Cyclic voltammograms for the electropolymerization of 10 mM EDOT and 10 mM (a) Cs[1]-Cl_2; (b) Cs[1]-Cl_4; (c) Cs[1]-Cl_6; (d) Cs[1]-I_6; and (e) PSS.

The key electrochemical reactions which lead to polymerization occur between +1.2 and +1.65 V (*vs.* Ag/AgCl) with a monomer oxidation onset potential at +1.3 V in the anodic scan of the first cycle (Fig. 1). Using the halo-derivatives as the doping agents delays the onset of electropolymerization by +0.2 V with regard to [1].[6] Essentially, for every sample there are two anodic peaks, a prominent and intense peak corresponding to polymer formation and a negative shoulder peak corresponding to the $Co^{3+/2+}$ redox process. The former occurs at +0.7, +0.6, +0.3 and +0.4 V *vs.* Ag/AgCl with a shift of 0.2, 0.1, 0 and −0.2 with consecutive cycles for PEDOT:[1]-Cl_2, PEDOT:[1]-Cl_4, PEDOT:[1]-Cl_6 and PEDOT:[1]-I_6, respectively, while the latter occurs at −0.2 V for PEDOT:[1]-Cl_2 and at −0.3 V for the remaining ones. On the other hand, the cathodic peaks are at the same positions of −0.5, 0 and +0.65 V *vs.* Ag/AgCl for PEDOT:[1]-Cl_2 and PEDOT:[1]-Cl_4 while for PEDOT:[1]-Cl_6 the

Table 1 Electrochemical parameters of the redox couple $Co^{3+/2+}$ for different COPs during polymerization

Sample ($Co^{3+/2+}$)	E_{pa} (V *vs.* Ag/AgCl)	E_{pc} (V *vs.* Ag/AgCl)	$E_{1/2}$ (V *vs.* Ag/AgCl) COP formation	$E_{1/2}$ (V *vs.* Ag/AgCl)
PEDOT:[**1**]-Cl_2	−0.2	−0.5	−0.35	−1.04
PEDOT:[**1**]-Cl_4	−0.3	−0.5	−0.40	−0.85
PEDOT:[**1**]-Cl_6	−0.3	−0.8	−0.55	−0.81
PEDOT:[**1**]-I_6	−0.3	−0.9	−0.6	−0.46

peaks are at −0.8 and −0.3 V and at −0.9 and −0.1 V for PEDOT:[**1**]-I_6. The electrochemical parameters for the redox couple $Co^{3+/2+}$ during the polymerization process for different COPs are listed in Table 1. The mechanism for polymerization can be speculated as the oxidation of the monomer generating a radical that could lead to polymer formation by the release of a proton.[2]

Fig. 1e shows the voltammogram recorded during the potentiodynamic synthesis of PEDOT:PSS in water. The onset potential was +0.6 V, with an increase in current for every cycle indicating the formation of the polymer on the electrode surface with an anodic peak at +0.7 V *vs.* Ag/AgCl. The voltammogram also showed a high and relatively constant capacitive current for PEDOT:PSS. The as-synthesized COPs were characterized using various spectroscopic and microscopic techniques (refer to the ESI† for further details).

The as-synthesized COPs were characterized using various spectroscopic and microscopic techniques. The morphology studies were carried out using the SEM technique (Fig. 2). It was observed that PEDOT:[**1**]-Cl_2 and PEDOT:[**1**]-Cl_4 consisted of small aggregates of rough spheres with dimensions around 5.5 and 4.5 μm, respectively. Interestingly, the morphology of PEDOT:[**1**]-Cl_6 was quite similar to the one observed for PEDOT:M[**1**] (M = Cs^+, Na^+, Li^+ and H^+),[30] small spheres with dimensions of 2.0 μm. In contrast, PEDOT:[**1**]-I_6 had a very distinct morphology in comparison to the others. The reference sample, PEDOT:PSS, also had a distinct morphology owing to the fact that the doping agent was a polymer instead of a 3D inorganic moiety.

To reinforce the success of electropolymerization, EDX analysis was also performed on the samples to estimate the elemental composition in each of them. The characteristic elements for PEDOT and metallacarboranes are S and Co, respectively. Hence, the ratio of S/Co would provide information regarding the stoichiometry as well as the extent of doping in each sample. Table 2 shows the ratio of S/Co for all the samples and it can be noticed that for every [**1**]-Cl_x, there are 1.5 molecules of PEDOT whereas for [**1**]-I_6 there are 2.6.

XPS analysis was also performed for the samples and compared with [**1**] as shown in Fig. 3. The results indicate the formation of a COP with the presence of different elements as shown in Table 3. Interestingly, the ratios of S/Co obtained from EDX and XPS analyses are different which hints at a difference in the surface and bulk composition of the newly synthesised COPs attributed to the difference in sample preparation and history of the sample. In the bulk due to the presence of more PEDOT, [**1**] participates more actively in the surface processes than in the internal processes. Thus, in the reduction process, metallacarborane is removed, resulting in a higher PEDOT ratio[25b] [for further details refer to the ESI].†

Electrochemical properties of PEDOT:[1]-X (X = Cl_x, x = 2, 4 and 6; I_6) and PEDOT:PSS

The electrochemical properties of PEDOT:[**1**]-X and PEDOT:PSS were investigated in 0.1 M Na_2SO_4 in water. Fig. 4 shows the

Table 2 Ratio of S/Co atomic % (S from PEDOT and Co from metallacarborane) of the samples PEDOT:[**1**]-Cl_x and PEDOT:[**1**]-I_6 by EDX analysis

Sample	S/Co (% At)
PEDOT:[**1**]-Cl_2	1.55 ± 0.10
PEDOT:[**1**]-Cl_4	1.55 ± 0.09
PEDOT:[**1**]-Cl_6	1.54 ± 0.21
PEDOT:[**1**]-I_6	2.56 ± 0.31

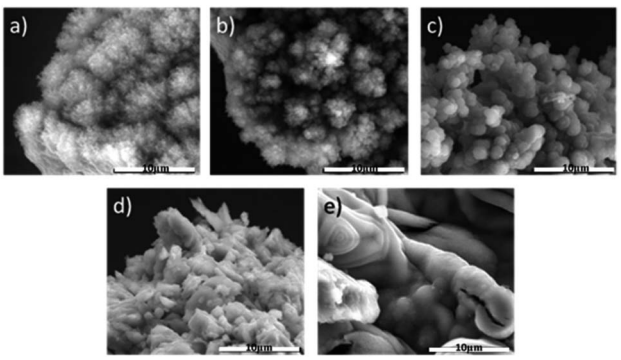

Fig. 2 Scanning electron microscope images of (a) PEDOT:[**1**]-Cl_2; (b) PEDOT:[**1**]-Cl_4; (c) PEDOT:[**1**]-Cl_6; (d) PEDOT:[**1**]-I_6; and (e) PEDOT:PSS at 500× with a 10 μm scale.

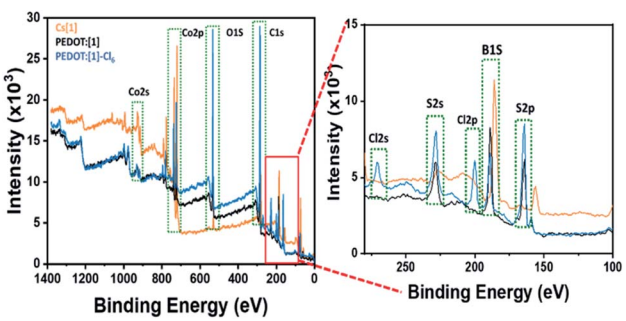

Fig. 3 XPS analysis of Cs[**1**], PEDOT:[**1**] and PEDOT:[**1**]-Cl_6 with the corresponding elements.

Table 3 Atomic % concentrations on the surface of different samples from XPS analysis

Sample	C	B	Cl	Co	S
[1]	31.28	66.63	—	3.57	—
PEDOT:[1]	59.89	18.41	—	0.89	4.72
PEDOT:[1]-Cl_6	62.72	10.95	2.98	0.57	5.03

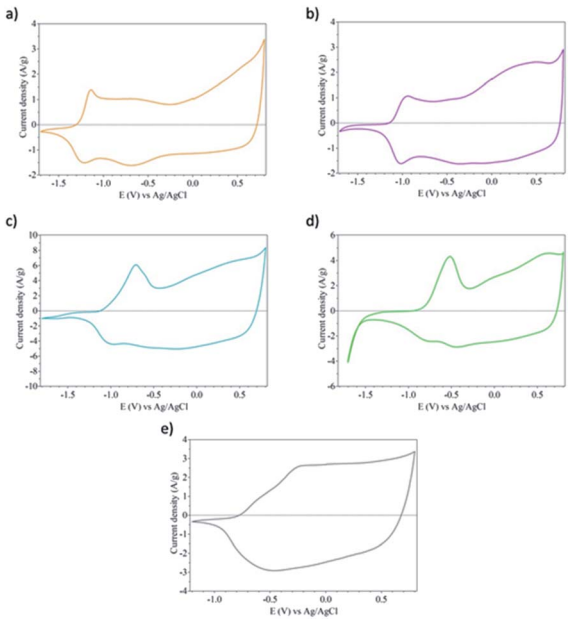

Fig. 4 Cyclic voltammograms for the electrochemical characterization of (a) PEDOT:[1]-Cl_2; (b) PEDOT:[1]-Cl_4; (c) PEDOT:[1]-Cl_6; (d) PEDOT:[1]-I_6; and (e) PEDOT:PSS in 0.1 M Na_2SO_4 at 100 mV s^{-1}.

stability window of different polymers with a scan rate of 100 mV s^{-1}. The redox peaks for the couple, $Co^{3+/2+}$, of [1]-Cl_2, [1]-Cl_4, [1]-Cl_6 and [1]-I_6 were found at −1.17, −0.97, −0.83 and −0.65 V, respectively, which confirms the presence of metallacarborane in the polymer matrix. In all the samples, a negative shift of the redox potential of the PEDOT:[1]-X polymers in comparison to the native values of the parent metallacarboranes was observed.

The second redox process that occurs corresponds to PEDOT. However, due to the overlap of the redox processes between the couple, $Co^{3+/2+}$, and PEDOT, only the peaks due to [1]-X are observable. This can be attributed to the fact that the metallacarboranes contribute to the faradaic current whereas PEDOT with a doping agent is capacitive. The specific capacitance values of the different COPs are shown in Table 4. Among the polymers, PEDOT:[1]-Cl_6 has the highest capacitive value of 326 F g^{-1}, around 2–3 times higher than the rest, including PEDOT:PSS. As mentioned earlier, [1]-Cl_6 is the only metallacarborane which shows a synergy between the electropolymerization of PEDOT and the $Co^{3+/2+}$ couple. Remarkably, this composite shows a specific capacitance value similar to that of PEDOT/ferrocene, thereby rendering it a good candidate for supercapacitors.[33] Furthermore, the as-synthesized PEDOT:PSS also had values very close to the reported ones,[34] suggesting that the potentiodynamic synthesis of the polymer is indeed effective and practical.

The linear sweep voltammograms of the samples in 0.1 M Na_2SO_4 at 0.5 mV s^{-1} show that the higher the number of B–Cl bonds in metallacarborane, the higher the overoxidation resistance limit (ORL) (Fig. S5†). Moreover, PEDOT:[1]-Cl_6 has a shoulder at +1.15 V which can be ascribed to the interplay between metallacarborane and PEDOT growth suggesting that [1]-Cl_6 delays the ORL in the polymer matrix. Notably, at different scan rates the LSV varies as will be seen in the following catalysis section.

The conductivity studies also suggest that synergy is most experienced in PEDOT:[1]-Cl_6 as it has the highest electrical in-plane conductivity among the polymers. The general range for the conductivity lies between 210 and 284 S cm^{-1} (Table 4). The different values of conductivity indicate a deep synergy between each doping agent and the polymer, and consequently the properties thereof. The trend is also in agreement with the conclusion that the higher the chloro-content in the doping agent, the higher the anodic potential of metallacarborane and hence, the higher the electrical conductivity. Table 4 also indicates that the conductivity of each of the samples is twice that of PEDOT:PSS.

Ionic conductivity by electrochemical impedance spectroscopy (EIS) of PEDOT:[1]-X (X = Cl_x, x = 2, 4 and 6; I_6) and PEDOT:PSS

In practice, the as-synthesized COPs require ionic conduction perpendicular to the membrane. In this regard EIS measurements were performed at different temperatures between 20 and 160 °C on a frequency scale from 0.1–10 MHz. The real part of the conductivity was analysed in terms of the corresponding Bode diagrams,[35] where conductivity varies with frequency for

Table 4 Values for the electrical parameters of PEDOT:[1]-X and PEDOT:PSS

Sample	C_s[a] [F g^{-1}]	σ^b [S cm^{-1}]	σ^c [60 °C, 10^{-3} S cm^{-1}]	σ^c [120 °C, 10^{-3} S cm^{-1}]	σ^c [160 °C, 10^{-3} S cm^{-1}]
PEDOT:[1]-Cl_2	106 ± 12	230 ± 15	6.3 ± 0.2	17 ± 1	13 ± 0.5
PEDOT:[1]-Cl_4	114 ± 14	248 ± 23	13 ± 0.3	20 ± 2	18 ± 0.6
PEDOT:[1]-Cl_6	326 ± 10	284 ± 22	26 ± 0.5	28 ± 2	22 ± 1
PEDOT:[1]-I_6	183 ± 11	252 ± 25	1.6 ± 0.1	2.3 ± 0.3	1.5 ± 0.1
PEDOT:PSS	175 ± 18	210 ± 37	1.5 ± 0.1	2.0 ± 0.1	2.4 ± 0.1

[a] Specific capacitance values. [b] Electrical conductivity measured in-plane in S cm^{-1} by the four-probe method. [c] Ionic conductivities at 60 °C, 120 °C and 160 °C.

all the membranes under dry conditions (Fig. S6†). Although the dielectric conductivity measurements (σ_{dc}) are easier to obtain by using Bode plots when the real part of the conductivity is constant and the phase angle is zero, σ_{dc} was observed from the Nyquist diagram for the sample PEDOT:[**1**]-Cl_2 as shown in Fig. S7.† Both diagrams, Bode and Nyquist, indicate that the behavior of PEDOT:[**1**]-Cl_2 is similar to a typical conductor material, at every temperature, where the real part of the impedance corresponding to the material resistance is constant, and the imaginary part is very small.

It can be observed that the real part of the conductivity for all the samples is constant for all ranges of temperature, which is a typical behaviour for a conductive material. For all the temperatures studied, the conductivity values increase with temperature as σ'PEDOT:[**1**]-Cl_6 > σ'PEDOT:[**1**]-Cl_4 > σ'PEDOT:[**1**]-Cl_2 > σ'PEDOT:[**1**]-I_6 ~ σ'PEDOT:PSS (Table 4). As expected, PEDOT:[**1**]-Cl_6 is the most conductive, which is also in accordance with the in-plane electrical conductivity measurements performed using the four-probe method. The conductivity values observed are higher than those observed for mixtures of zwitter ionic liquids (ZILs) and $LiNTf_2$ or even for the cross-linked polymeric ionic-like liquids (SILLPs).[36,37]

The conductivity σ' is characterized by a plateau independent of the frequency and the value is virtually constant corresponding to direct-current conductivity (σ_{dc}) of the sample. The lack of any deviation from the σ_{dc} in the low range frequencies due to the electrode polarization (EP) resulting from the blocking of the electrodes suggests that EP is absent in these materials.

Fig. S8† shows the conductivity values for all the samples as a function of temperature. From the plot, we can observe that polymers with metallacarboranes as doping agents follow a typical Arrhenius behavior with two distinct traits, one between 20 °C and 120 °C where the conductivity increases with increasing temperature in accordance with the Arrhenius equation (eqn (1)) and the second from 120 °C where the conductivity decreases. The exception to the observed trend is PEDOT:PSS, where the tendency is linear for all ranges of temperature. This anomaly in the conductivity where there is temperature dependency of mobile ions particularly at higher temperatures where conductivity begins to fall sharply is difficult to explain but is presumably due to solvent evaporation leading to membrane dehydration or can be associated to the variation in Debye's length as previously reported.[38]

$$\ln \sigma_{dc} = \ln \sigma_{\infty} - \frac{E_{act}}{RT} \quad (1)$$

Following eqn (1), the activation energy for each of the samples was calculated from the slopes by fitting the region 20–120 °C. The trend observed is as follows: E_{act}(PEDOT:[**1**]-Cl_6) < E_{act}(PEDOT:[**1**]-Cl_4) ~ E_{act}(PEDOT:PSS) < E_{act}(PEDOT:[**1**]-I_6) < E_{act}(PEDOT:[**1**]-Cl_2). Reinforcing the previous discussions, E_{act}(PEDOT:[**1**]-Cl_6) has the lowest activation energy. Our results show that all compounds display activation energies lower than those of Nafion membranes (10.5 kJ mol^{-1})[39] and significantly smaller than previously reported values for polycrystalline salts of CsH_2PO_4 (38.6 kJ mol^{-1})[40] in the same temperature ranges. Interestingly, the values obtained are quite similar to powders of Na[**1**], Li[**1**] and H[**1**] which were 7.8, 7.9 and 5.6 kJ mol^{-1}, respectively.

To further analyze the differences in the conductivity and activation energy, we express the temperature dependence of conductivity in terms of Eyring's absolute rate theory as:

$$\sigma = C_0 T \exp\left(-\frac{\Delta G^{**}}{RT}\right) \quad (2)$$

Eqn (2) constitutes an Arrhenius law in which $\Delta G^{**} = \Delta H^{**} - T\Delta S^{**}$ has been taken into account with C_0 being the pre-factor dependent on frequency, ΔG^{**} being the activation Gibbs free energy of the microscopic conduction process in the sample, and ΔS^{**} being related to the thermodynamic excess of entropy associated with the macroscopic structural changes of the material that give rise to entropic restrictions during the motion of the charge carriers. ΔH^{**} is the enthalpy change associated with the conduction process, T is the absolute temperature and R is the universal gas constant.

Since the charge transport is thermally activated, the energy ΔG^{**} involves the formation of an activated complex linked to ion hopping. The values of ΔH^{**} and ΔS^{**} can be obtained from the slope and T-intercept of the plot $\ln(\sigma/T)$ *vs.* $1000/T$, respectively (Fig. S9†). The calculated values of these quantities are shown in Table 5. They are associated with conductivity through ΔH^{**} and the structural changes through ΔS^{**}. From the data, it can be concluded that for most of the samples the ΔH^{**} decreases and ΔS^{**} increases with an increase in the number of Cl atoms in the doping agent. The activation enthalpy and entropy are rather similar for PEDOT:[**1**]-Cl_6 and PEDOT:[**1**]-Cl_4 while for PEDOT:[**1**]-Cl_2, they are different which can be attributed to the abrupt change observed from 60–80 °C.

Comparison of the oxygen evolution reaction of PEDOT:X films deposited on glassy carbon electrodes; X = PSS, [1], and [1]-Cl_6

The investigations reported in this work have shown that [**1**] and its halogenated derivatives [**1**]-Cl_x (x = 2, 4 and 6) and [**1**]-I_6, serving as redox reversible active dopant agents of PEDOT have improved, among others, the electrical properties of pristine PEDOT:PSS. An exciting aspect was observed as shown in Fig. 4a–c that [**1**] and its chlorinated derivatives had their pristine redox properties altered as a consequence of the PEDOT matrix in which they were embedded and these had moved

Table 5 Values for the energies calculated for all the samples with the reference, PEDOT:PSS, for comparison

Sample	E_{act} [kJ mol^{-1}]	ΔH^{**} [kJ mol^{-1}]	ΔS^{**} [J mol^{-1} K^{-1}]
PEDOT:[**1**]-Cl_2	14.1 ± 1.4	13.6 ± 1.4	−1.5 ± 0.2
PEDOT:[**1**]-Cl_4	6.5 ± 0.6	3.7 ± 0.3	−34.7 ± 2.5
PEDOT:[**1**]-Cl_6	5.1 ± 0.8	2.4 ± 0.3	−33.3 ± 2.4
PEDOT:[**1**]-I_6	10.2 ± 1.0	7.4 ± 0.5	−42.7 ± 3.1
PEDOT:PSS	6.2 ± 0.3	3.2 ± 0.2	−54.9 ± 3.4

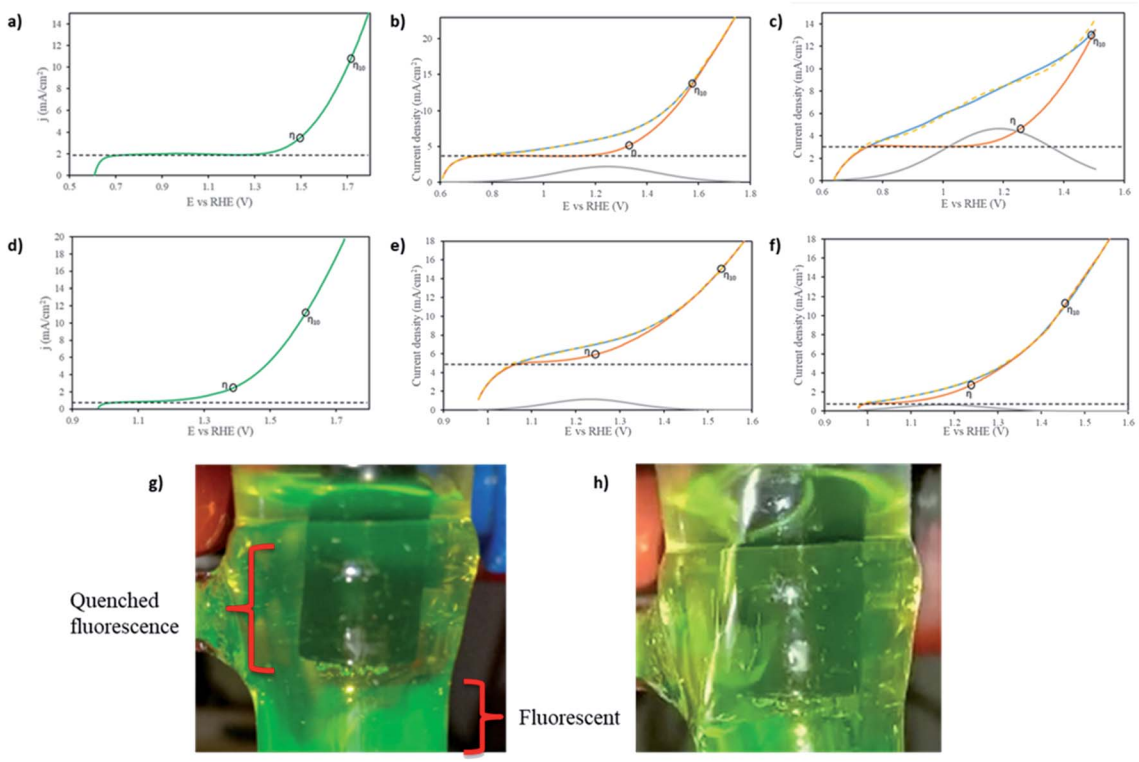

Fig. 5 Linear sweep voltammetry during WOC activity with deconvolution of capacitive current + catalysis $Co^{4+/3+}$ oxidation and PEDOT:PSS voltammograms. The original voltammogram in blue, deconvoluted capacitive current and catalytic activity in orange, deconvoluted $Co^{4+/3+}$ oxidation, calculated voltammogram in yellow dotted and capacitive current in black dotted. (a) PEDOT:PSS at pH = 7, (b) PEDOT:Cs[*o*-COSAN] at pH = 7, (c) PEDOT:Cs[Cl_6-*o*-COSAN] at pH = 7, (d) PEDOT:PSS at pH = 13, (e) PEDOT:Cs[*o*-COSAN] at pH = 13 and (f) PEDOT:Cs[$C1_6$-*o*-COSANI] at pH = 13; (g) quenching of fluorescein fluorescence (encircled) due to O_2 evolution; (h) bubbling of N_2 to remove the O_2 formed and hence the recovery of fluorescein fluorescence.

towards more anodic values. These observations were corroborated by the traces in Fig. S5a–d,† and we thought that if the $Co^{3+/2+}$ couple shifts to more positive values, might not the $Co^{4+/3+}$ couple be more accessible? This motivated us to see if the broadly accepted poor electrocatalytic properties of PEDOT:PSS in the oxidation of water to O_2 would be significantly improved by substituting non-redox PSS with a redox tunable metallacarborane like [**1**] and its halogenated derivatives [**1**]-Cl_x. The water oxidation catalysis results are shown in Fig. 5. The electrochemically active surface area (ECSA) as well as the roughness factor (RF) were calculated for PEDOT:[**1**] and PEDOT:[**1**]-Cl_6 as shown in Table 6.

It is noteworthy that in all cases when the *I*/*V* trace experiences a significant change in the slope, O_2 release is observed. Due to the dark color of PEDOT/X, the formation of bubbles on the material is not observed, but their subsequent evolution is clear after a few seconds due to the abrupt change in the *I*/*V* slope. Furthermore, $Co^{4+/3+}$ oxidation was deconvoluted from the original voltammograms shown in Fig. S10,† separating this oxidation wave (parameters found in Table S2†) from the curve that contains both the capacitive current and the catalytic curve. O_2 was identified as the gas evolved, which was proven by the quenching of fluorescein by the generated O_2 as shown in Fig. 5 and S11†.[41,42]

The relative overpotential (η_{10})[43] is measured as the potential difference (voltage) between the oxidation potential E_{10} at which a current of 10 mA is determined for PEDOT:PSS and the voltage, *E*, at which such current is found for PEDOT:[**1**], and PEDOT:[**1**]-Cl_6. These values are shown in Table 7.

Table 7 shows the overpotential values which are negative because they are compared to PEDOT:PSS which is the one for which the improvement is intended. η_{10} values were obtained directly from the original voltammograms while η values were extrapolated using the deconvoluted catalytic curves by intersecting the line of the capacitive current with the tangent of the catalytic wave. These η values are −250 and −160 mV at pH = 7 and −150 and −140 mV at pH = 13 (*vs.* PSS), for [**1**]-Cl_6 and [**1**], respectively. It is noteworthy that E_{10} is 1.32 V, only 0.09 V away from the thermodynamic value of 1.23 V. All this is consistent with the title that states "*How to switch from a poor PEDOT:X oxygen evolution reaction (OER) to a good one.*"

Table 6 Values of ECSA and RF for the samples, PEDOT:[**1**] and PEDOT:[**1**]-Cl_6 at pH = 7 and pH = 13

	pH = 7		pH = 13	
Sample	ECSA (cm^2)	RF	ECSA (cm^2)	RF
PEDOT:[**1**]	1.013	144.7	1.020	145.8
PEDOT:[**1**]-Cl_6	0.716	102.3	1.030	147.2

Table 7 Values for η_{10} and η obtained for PEDOT:PSS, PEDOT:Cs[**1**] and PEDOT:Cs[**1**]-Cl_6 in order to compare the water oxidation catalytic power

	pH = 7			pH = 13		
Sample	E_{10} [V]	η_{10}	η_{10} *vs.* PSS	E_{10} [V]	η_{10}	η_{10} *vs.* PSS
PEDOT:PSS	1.722	0.492	0	1.602	0.372	0
PEDOT:[**1**]	1.599	0.369	−0.123	1.503	0.273	−0.099
PEDOT:[**1**]-Cl_6	1.489	0.259	−0.233	1.453	0.223	−0.149
	pH = 7			pH = 13		
Sample	E [V]	η	η *vs.* PSS	E [V]	η	η *vs.* PSS
PEDOT:PSS	1.496	0.266	0	1.387	0.157	0
PEDOT:[**1**]	1.336	0.106	−0.16	1.245	0.015	−0.142
PEDOT:[**1**]-Cl_6	1.248	0.018	−0.248	1.24	0.01	−0.147

Discussion

As the name indicates, conducting organic polymers (COPs) are predominantly current conducting but they also have an electrochemical response that results in a dependence of the current on the applied potential, producing a redox process. In general, in the reduced form, they do not carry current and in the oxidized form they do, although the current decreases at high oxidation potentials due to over-oxidation phenomena that deteriorate the conjugated electronic system. When they are in the oxidized form, *i.e.*, conductive, they require anions to compensate for the positive charges generated in the polymer. Therefore, this relates electrical conduction to the redox phenomena, but refers only to the polymer itself. Can this conductivity be modified by the redox properties of the doping agent? The answer is yes, as we have demonstrated. In almost all existing COPs the dopant is not redox active; an example is PSS that is a typical dopant of PEDOT. Hence, in this work on PEDOT we have used PSS as a reference polymer, PEDOT:PSS. As we have pointed out in the introduction, redox polymers are those that change their electrochemical properties with a change in the oxidation state that must be reversible. We expected that the coexistence of two relevant electroactive species, the COP itself and a well-defined redox reversible dopant, in the same polymer, would lead to a remarkable synergy, and indeed it did. To achieve this, we have used molecules almost identical in volume with a common scaffold,[44,45] $[Co(C_2B_9H_{11})_2]^-$ ($[\mathbf{1}]^-$), as doping agents. In this way, we can ensure that the internal structure of the polymers was not affected. The difference between the doping agents lies in the number of substituents and their nature, grossly Cl and in one case I, [**1**]-Cl_x (x = 2, 4 and 6) and [**1**]-I_6. All substituents are in a second sphere of influence to the metal. In this manner, the value of $E_{1/2}$ has been modulated. The higher the number of halogens, the more positive the $E_{1/2}$ is, approaching or overlapping the range of potentials in which there is a current associated with the voltage in the PEDOT/PSS reference system. However, which are the physical properties in which the synergism between the two redox systems is observed? The first property where synergy can be seen is in the electropolymerisation process. The area within the I/V curve is much larger for PEDOT:[**1**]-Cl_6 than for the others, with PEDOT:[**1**]-I_6 being the second largest, followed by PEDOT:[**1**]-Cl_4 and PEDOT:[**1**]-Cl_2. Interestingly, the negative current is very prominent in the potential zone close to the cathodic peak of PEDOT:[**1**]-Cl_6. A comparison of PEDOT:[**1**]-Cl_6 with the reference PEDOT:PSS shows a large difference in the morphology and area of the two, expressing the relevance of the redox activity of the doping agent and its $E_{1/2}$. This was with regard to electropolymerization alone, but what about the CV of these materials in water with one electrolyte, in our case Na_2SO_4. The study of their capacitance (C) indicates that C parallels with the $E_{1/2}$ of [**1**]-Cl_x. In this manner, the C data follow the order PEDOT:[**1**]-Cl_6 > PEDOT:[**1**]-I_6 ≈ PEDOT:PSS > PEDOT:[**1**]-Cl_4 ≈ PEDOT:[**1**]-Cl_2. The relationship between electrochemical behavior and $E_{1/2}$ has been clearly reflected in the two previous experiments. Due to their nature, an electrolyte was required in all of the studies; however, we have already mentioned that the characteristic of a COP was the electrical conductivity and have already shown that there is a relationship between electrical conductivity and electrochemical behavior. This has been evidenced by the study of in-plane electrical conductivity. The same pattern of behavior observed between electrochemical performance and $E_{1/2}$ has been reproduced in this case. If the former was true the trend PEDOT:[**1**]-Cl_6 > PEDOT:[**1**]-I_6 ≈ PEDOT:[**1**]-Cl_4 > PEDOT:[**1**]-Cl_2 was expected, as indeed it occurs. Noticeably, electrochemically synthesized PEDOT:PSS was the least conducting, but it was in-fact more conductive than commercial PEDOT:PSS. Interestingly, the ionic conductivity also follows a comparable trend, σ'PEDOT:[**1**]-Cl_6 > σ'PEDOT:[**1**]-Cl_4 > σ'PEDOT:[**1**]-Cl_2 > σ'PEDOT:[**1**]-I_6 ∼ σ'PEDOT:PSS. However, when it is represented by activation energy E_a and ΔH^{**}, even with slight alterations, we note that larger conductivities relate to a smaller E_a and ΔH^{**}; E_a follows the trend PEDOT:[**1**]-Cl_6 < PEDOT:PSS ≈ PEDOT:[**1**]-Cl_4 < PEDOT:[**1**]-I_6 < PEDOT:[**1**]-Cl_2.

Hereby the position of PEDOT:[**1**]-I_6 has changed with respect to the position it occupied in the in-plane conductivity, but this is not strange considering that in the case of ionic conductivity the size of the ions is important and therefore there is no doubt that with the same number of substituents the iodinated derivative is larger than the chlorinated one, which explains the possible change of position. As indicated above, the dopant has approximately the same volume if the nature of the substituent(s) is the same or very similar, as has been observed in crystals that can be considered as solid solutions. Therefore, the stability of the material can also be related to $E_{1/2}$ in case the stability of the material increases as $E_{1/2}$ approaches the center of the redox transition of the polymer. If we look at the degradation curves as a function of T, analyzed by TGA (Fig. S4†), we see that the most stable one is PEDOT:[**1**]-Cl_6 > PEDOT:[**1**]-Cl_4 > PEDOT:[**1**]-Cl_2 > PEDOT:PSS. An identical order of stability is observed by checking the stability by linear sweep voltammetry, therefore relating thermal stability and electrochemical stability to $E_{1/2}$ as the number of monomers in the polymer and the number of doping

agents per monomer varies with the substituents; PEDOT:[**1**]-Cl_6 ≈ PEDOT:[**1**]-Cl_4 ≈ PEDOT:[**1**]-Cl_2 show a monomer : doping agent ratio of 3 : 2, whereas for PEDOT:[**1**]-I_6 the ratio is 5 : 2.

In all these experiments we have seen how a redox active doping agent has been able to modify the properties of a COP. The question for us was can it be that a COP alters the properties of the doping agent? We have previously indicated that most probably the $E_{1/2}$ of the $Co^{3+/2+}$ couple was changed towards more affordable reduction values. Could it be that the $Co^{4+/3+}$ pair also modified towards more accessible oxidation values? A good experiment to ascertain this, as well as having enormous energy and environmental relevance, was the splitting of water into O_2 and H_2. In our case, we have focused on the oxidation of water. Recently [**1**] has been used for the oxidation of alcohols by applying UV radiation, obtaining excellent results with a [**1**]: substrate ratio of 1 : 10 000.[46]

The redox couple to which the photocatalytic effect is attributed is $Co^{4+/3+}$. This motivated us to think that [**1**] could also act as an electrocatalyst. However, the redox potentials of the three redox couples in their pristine forms are: for $[Co(C_2B_9H_{11})_2]^{2-/3-}$ −2.29, for $[Co(C_2B_9H_{11})_2]^{1-/2-}$ −1.40 and for $[Co(C_2B_9H_{11})_2]^{0/1-}$ +1.56 with reference to Ag/AgCl, that correspond to $Co^{2+/1+}$, $Co^{3+/2+}$, and $Co^{4+/3+}$, respectively.[44] At first, the $Co^{4+/3+}$ value is outside the limits to be an interesting catalyst for water oxidation but if it is embedded in a polymeric matrix the $E_{1/2}$ could be more accessible. It is well known that secondary coordination sphere interactions can fine tune the E° within proteins that share similar primary coordination spheres by values ranging 500 mV, and hydrogen-bonding network around the metal center is also a prominent factor in tuning the E°.[47–49]

[**1**] has a high capacity to form hydrogen and dihydrogen bonds and therefore it was possible that its E was influenced within the PEDOT matrix, increasing its electrocatalytic capacity, as shown in the results above. So, we wanted to demonstrate that [**1**] has influenced the properties of PEDOT but surprisingly, PEDOT also has influenced the properties of [**1**]. The combination of two elements, that would not be suitable to produce very acceptable values of overpotential (η) in the oxidation of water separately, by synergy generates a material that demonstrates the possibility to convert a bad catalyst for the oxidation of water into a 'good one' that shows very interesting possibilities.

Experimental section

Chemicals required

3,4-Ethylenedioxythiophene (EDOT) and sodium poly(-styrenesulfonate) (PSS) were purchased from Sigma-Aldrich and used without further purification. Cs[**1**] was obtained from Katchem Spol.sr.o which was halo-derivatized following reported procedures[23,49–53] and characterized (refer to the ESI for further details).†

Electro-polymerization of PEDOT:[1]-X (X = Cl_x, x = 2, 4 and 6; I_6) and PEDOT:PSS

The electro-polymerization of PEDOT with metallacarboranes was performed using a potentiostat/galvanostat AutoLab PGSTAT302N by the technique of cyclic voltammetry at room temperature using an in-house one compartment three electrode cell. The system consisted of glassy carbon as the working electrode, Ag/AgCl (3 M KCl) as the reference electrode and Pt wire as the counter electrode. All the electrodes were polished prior to use to ensure the removal of any oxidative layer. Electropolymerization involved using 10 mM Cs[**1**]-X with 10 mM EDOT in dry acetonitrile in a potential range of −1.3 to +1.65 V *vs.* Ag/AgCl with a scan rate of 50 mV s^{-1} for 20 cycles. Similarly, the electro-polymerization of PEDOT:PSS was performed in water using the same concentrations of EDOT and PSS as before with a potential range of −1 to +1.5 V *vs.* Ag/AgCl, with the same scan rate and number of cycles.

The as-synthesized polymers were characterized using different techniques such as SEM, XPS, FTIR and TGA. SEM studies were performed in a SEM Quanta 200 FEG-ESEM coupled to an EDX spectrometer for the elemental analysis of S and Co, operating at an acceleration voltage of 15 kV and low vacuum of 50 Pa. The samples were prepared by deposition on a carbon tape. XPS measurements were performed at room temperature with a SPECS PHOIBOS 150 hemispherical analyzer (SPECS GmbH, Berlin, Germany) at a base pressure of 5 × 10^{-10} mbar using monochromatic Al Kα radiation (1486.74 eV) as the excitation source operated at 300 W. The energy resolution as measured by the FWHM of the Ag $3d_{5/2}$ peak for a sputtered silver foil was 0.62 eV. The FTIR spectra were recorded using a single-reflection ATR diamond crystal accessory in a JASCO FT/IR-4700 spectrometer between 600 and 4000 cm^{-1} with a resolution of 4 cm^{-1}. The thermal stability of the polymers was analysed using a NETZSCH-STA 449 F1 Jupiter apparatus. All samples were weighed in alumina crucibles and were heated in a nitrogen flow (40 mL min^{-1}) at a heating rate of 10 K min^{-1} from 298–1173 K.

Preparation of PEDOT:[1]-X (X = Cl_x, x = 2, 4 and 6; I_6) and PEDOT:PSS pellets

30–40 mg of the powdered compounds was finely pulverized using a mortar and pestle. The pulverized compounds were then subjected to a force of 10 tons for 2 minutes in a pellet-forming device to obtain the pellets for the conductivity studies.

Electrochemical studies

The electrochemical capabilities of the polymers were explored using cyclic and linear sweep voltammetry in a 3-electrode system. The polymer coated glassy carbon was used as the working electrode whereas Ag/AgCl and Pt wire were used as the reference and counter electrodes, respectively. The CV experiments were performed in 0.1 M $Na_2SO_{4(aq)}$ between −1.8 and +0.8 V *vs.* Ag/AgCl with a scan rate of 100 mV s^{-1} while the LSV experiments were performed at 0 to +1.5 V *vs.* Ag/AgCl with a scan rate of 0.5 mV s^{-1}, also using 0.1 M $Na_2SO_{4(aq)}$.

Calculating the electrochemically active surface area

The electrochemically active surface area (ECSA) is calculated by dividing the double layer capacitance (C_{DL}) of the impregnated electrode by the specific capacitance (C_s) of the impregnated

material in the electrode. With this relationship, the ECSA is obtained (eqn (3)). The C_{DL} of the different systems was estimated using CV. A 0.1 V non-faradaic window was chosen from the LSVs, where no redox processes occur, and all the measured current is due to double-layer charging. Based on this assumption, the i can be calculated as the product of the electrochemical C_{DL} and the scan rate (ν) (eqn (4)). Plotting i as a function of ν yields a straight line with a slope equal to C_{DL}, both in oxidative and reductive currents. In this manner, 5 different scan rates were used (5, 25, 50, 75 and 100 mV s^{-1}), holding the working electrode at each potential vertex for 10 seconds before the next step (Fig. S10†). Once C_{DL} was obtained, it was divided by the C_s of PEDOT:PSS.

$$\mathrm{ECSA} = \frac{C_{DL}}{C_s} \tag{3}$$

$$i = \nu C_{DL} \tag{4}$$

Conductivity studies using the four-probe method

The electrical conductivity of the samples was measured using the four-probe method, having them electro-deposited on ITO substrates. The measurements were repeated three times to ensure reproducibility. The sample thickness was measured using a profilometer.

Electrochemical impedance (EIS) studies

Impedance measurements were carried out for all the samples at distinct temperatures, from 293–473 K, with a frequency window of $10^{-1} < f < 10^{7}$ Hz. The experiments were performed at 100 mV amplitude, using a Novocontrol broadband dielectric spectrometer (Hundsangen, Germany) integrated with an SR830 lock-in amplifier with an alpha dielectric interface. Experimentally, 100 mV was chosen as the appropriate voltage to attain a linear response. Thus, two gold electrodes were attached to both sides of the sample by co-pressing the synthesized COPs in a sandwich cell configuration. The EIS measurements were performed following reported procedures.[54,55]

Briefly, the assembled membrane-electrode was annealed in the Novocontrol setup under an inert N_2 atmosphere. The measurements were carried out in two temperature cycles wherein, in the first cycle the temperature was increased from ambient temperature to 473 K and then lowered to 293 K, while in the other cycle the temperature was increased from 293 to 473 K, both in steps of 20 K with the measurement of the dielectric spectra.

Water oxidation catalysis

PEDOT films were electrochemically made and deposited on the flat surface of a glassy carbon electrode, as described above, and doped with the representative doping anions, PSS, [**1**], and [**1**]-Cl_6, leading to the formation of PEDOT:PSS, PEDOT:[**1**], and PEDOT:[**1**]-Cl_6, respectively. These were then set in a three electrode system having the doped-PEDOT coated glassy carbon as the working electrode, Ag/AgCl as the reference electrode and Pt wire as the counter electrode with 0.1 M KNO_3 for pH = 7 and 0.1 M NaOH for pH = 13 as the electrolytes. The studies were carried out at a neutral pH and at pH 13. The materials were studied by applying precisely the same conditions to all, and the current was measured against an increasing anodic voltage in order to have an accurate comparison of all the three materials, with PEDOT:PSS as the reference. Linear sweep voltammetries were deconvoluted by taking the PEDOT:PSS curve fitted to the PEDOT:X curves where $Co^{4+/3+}$ oxidation was deconvoluted using the solver function of Microsoft Excel 2018 in order to fit the oxidation Gaussian function (eqn (S1)†) in the original curve.

Conclusions

With this work, we aimed to study the synergistic effect between two intimately blended, highly stable and reversible redox active components, the θ shaped 3D aromatic metallacarborane and PEDOT, with particular interest in the water oxidation reaction. $[Co(C_2B_9H_{11})_2]^-$, being the most stable representative, and its halo-derivatives, [**1**]-Cl_x (x = 2, 4 and 6) and [**1**]-I_6, were chosen as the redox doping agents. To obtain charge neutrality while avoiding excessive domains of opposite charges in the polymer as homogenously as possible, the composite was synthesized by electropolymerization with a monovalent doping anion. Even though anions such as ferro/ferricyanide or POMs fulfill the requirements of stability and redox reversibility, the lack of a tunable $E_{1/2}$ and a high load of negative charge on a single spot make them less attractive compared to metallacarboranes. The metallacarborane discussed in this work, [**1**], can be halo-derivatized in a stepwise manner to yield anions with distinct $E_{1/2}$ values having lower charge densities. The reference PEDOT:PSS in aqueous 0.1 M Na_2SO_4 at 100 mV s^{-1} produces a capacitive response from −0.9 to +0.8 V *vs.* Ag/AgCl. Therefore, [**1**] and its halo derivatives, [**1**]-Cl_x (x = 2, 4 and 6) and [**1**]-I_6, are better suited to study the synergy between the redox reversible components of the dual redox materials.

The synergy is notably seen initially in the CV recorded during the preparation of the composite where a series of sequential snapshots for the evolution of each of the reagents are seen. Particularly, it is evident that over the course of time native [**1**] disappears and is integrated into the dual redox material. Hence, the native redox properties of metallacarboranes are altered when incorporated into the polymer matrix of PEDOT. Due to the synergy, it can be expected that the properties, particularly the electrochemical properties, of the dual redox material would not simply be an accumulation of each of the individual components, but rather a well-integrated one. An evidence for the synergy is that the CV recorded for the dual material which is radically different from that of the reference, PEDOT:PSS, and has intense peaks due to the doping agents but at different potentials from their native values. Remarkably, even though all the derivatives had their native $E_{1/2}$ values altered in the dual material, the differences between the values were similar to the ones observed for the doping agents

alone. The closer the native value of [**1**]-Cl_x to 0, which is the center of the capacitive curve for PEDOT:PSS, the more enhanced is the property observed. This is observed for specific capacitance studies where the trend followed for PEDOT:[**1**]-Cl_6 is $x = 2 < 4 < 6$, with 6 being the highest and two-fold higher than that for PEDOT:PSS. A similar trend is also observed for the conductivity, both electrical and ionic, studies where the reference has the lowest conductivity in comparison to the others. The activation energies agree with this trend as the charge transport is thermally activated.

Reciprocally, it has been shown that the properties of the dopant are modified by the polymer. Thus, due to its high $E_{1/2}$, the $Co^{4+/3+}$ couple would not be an efficient electrocatalyst for water oxidation but when it is immersed in the PEDOT matrix the $Co^{4+/3+}$ potential is more accessible, probably due to the secondary coordination sphere interactions and importantly the capacity of [**1**] to form hydrogen bonds with itself and with PEDOT so that very low overpotential values are obtained, which justifies the title of the work, *How to switch from a poor PEDOT:X oxygen evolution reaction (OER) to a good one*.

This work can be considered as an initial step towards better conducting materials with tunable redox potentials and enhanced electrochemical properties.

Author contributions

J. A. M. Xavier & I. Fuentes – formal analysis, investigation, methodology, visualization and writing – original draft, review & editing; M. Nuez-Martínez – data curation, investigation, validation and writing – review & editing; Z. Kelemen – data curation and investigation; A. Andrio – investigation and methodology; C. Viñas – project administration and resources, conceptualization, methodology, funding acquisition, supervision, and writing – original draft, review & editing; V. Compañ – investigation, visualization and writing review & editing. F. Teixidor – conceptualization, methodology, funding acquisition, supervision, and writing – original draft, review & editing.

Conflicts of interest

There are no conflicts to declare.

Acknowledgements

Jewel A. M. Xavier and Isabel Fuentes have contributed equally to this work. We gratefully acknowledge the Spanish Ministerio de Economía y Competitividad (PID2019-106832RB-I00) and Generalitat de Catalunya (2017SGR1720). Jewel A. M. Xavier acknowledges the DOC-FAM programme under the Marie Sklodowska-Curie grant agreement no. 754397. This work was also funded by the Spanish Ministry of Science, through the "Severo Ochoa" Programme for Centers of Excellence in R&D (CEX2019-000917-S). Jewel A. M. Xavier and Miquel N. M are enrolled in the PhD program of UAB.

Notes and references

1 Y. H. Ha, N. Nikolov, S. K. Pollack, J. Mastrangelo, D. B. Martin and R. Shashidhar, *Adv. Funct. Mater.*, 2004, **14**, 615.
2 (*a*) D. A. Mengistie, C. H. Chem, K. M. Boopathi, F. W. Pranoto, L. J. Li and C. W. Chu, *ACS Appl. Mater. Interfaces*, 2015, **7**, 94; (*b*) M. Ren, H. Zhou and H. J. Zhai, *J. Mater. Sci.: Mater. Electron.*, 2021, **32**, 10078.
3 A. V. Volkov, K. Wijeratme, E. Mitraka, U. Ail, D. Zhao, K. Tybrandt, J. W. Andreasen, M. Berggren, C. Crispin and I. Zozoulenko, *Adv. Funct. Mater.*, 2017, **27**, 1700329.
4 Y. Parl, J. Berger, Z. Tang, L. Müller-Meskamp, A. F. Lasagni, K. Vandewal and K. Leo, *Appl. Phys. Lett.*, 2016, **109**, 093301.
5 X. Wu, J. Liu and G. He, *Org. Electron.*, 2015, **22**, 160.
6 X. Wu, J. Liu, D. Wu, Y. Zhao, X. Shi, J. Wang, S. Huang and G. He, *J. Mater. Chem. C*, 2014, **2**, 4044.
7 A. Proust, B. Matt, R. Villanneau, G. Guillemot, P. Gouzerh and G. Izzet, *Chem. Soc. Rev.*, 2012, **41**, 7605.
8 P. Ma, F. Hu, J. Wang and J. Niu, *Coord. Chem. Rev.*, 2019, **378**, 281.
9 A. Blazevic and A. Rompel, *Coord. Chem. Rev.*, 2016, **307**, 42.
10 M. Misono, *Mol. Eng.*, 1993, **3**, 193.
11 I. V. Kozhevnikov, *Chem. Rev.*, 1998, **98**, 171.
12 P. Gómez-Romero, K. Cuentas-Gallegos, M. Lira-Cantú and N. J. Casañ-Pastor, *J. Mater. Sci.*, 2005, **40**, 1423.
13 X. X. Li, D. Zhao and S. T. Zheng, *Coord. Chem. Rev.*, 2019, **397**, 220.
14 J. Zhang, Y. Huang, G. Li and Y. Wei, *Coord. Chem. Rev.*, 2019, **378**, 395.
15 S. S. Wang and G. Y. Yang, *Chem. Rev.*, 2015, **115**, 4893.
16 Y. Wang and I. A. Weinstock, *Chem. Soc. Rev.*, 2012, **41**, 7479.
17 A. Banerjee, B. S. Bassil, G. V. Röschenthaler and U. Kortz, *Chem. Soc. Rev.*, 2012, **41**, 7590.
18 P. Yin, D. Li and T. Liu, *Chem. Soc. Rev.*, 2012, **41**, 7368.
19 H. N. Miras, J. Yang, D. L. Long and L. Cronin, *Chem. Soc. Rev.*, 2012, **41**, 7403.
20 H. Lv, Y. V. Geletii, C. Zhao, J. W. Vickers, G. Zhu, Z. Luo, J. Song, T. Lian, D. G. Musaev and C. L. Hill, *Chem. Soc. Rev.*, 2012, **41**, 7572.
21 M. Tarrés, V. S. Arderiu, A. Zaulet, C. Viñas, F. Fabrizi de Biani and F. Teixidor, *Dalton Trans.*, 2015, **44**, 11690.
22 T. C. Li, A. M. Spokoyny, C. She, O. K. Farha, C. A. Mirkin, T. J. Marks and J. T. Hupp, *J. Am. Chem. Soc.*, 2010, **132**, 4580.
23 P. Gonzalez-Cardoso, A. I. Stoica, P. Farras, A. Pepiol, C. Viñas and F. Teixidor, *Chem.–Eur. J.*, 2010, **16**, 6660.
24 M. J. Hardie and C. L. Raston, *Chem. Commun.*, 2001, **10**, 905.
25 (*a*) C. Masalles, J. Llop, C. Viñas and F. Teixidor, *Adv. Mater.*, 2002, **14**, 826; (*b*) S. Gentil, E. Crespo, I. Rojo, A. Friang, C. Viñas, F. Teixidor, B. Grüner and D. Gabel, *Polymer*, 2005, **46**, 12218.
26 M. Tarres, C. Viñas, P. Gonzalez-Cardoso, M. M. Hanninen, R. Sillanpaa, V. Dordovic, M. Uchman, F. Teixidor and P. Matejcek, *Chem.–Eur. J.*, 2014, **20**, 6786.

27 M. F. Hawthorne, D. C. Young, T. D. Andrews, D. V. Home, R. L. Pilling, A. D. Pitts, M. Reintjes, L. F. Warren and P. A. Wener, *J. Am. Chem. Soc.*, 1968, **90**, 879.
28 R. A. Wiesboeck and M. F. Hawthorne, *J. Am. Chem. Soc.*, 1964, **86**, 1642.
29 J. Poater, C. Viñas, I. Bennour, S. Escayola, M. Solà and F. Teixidor, *J. Am. Chem. Soc.*, 2020, **142**, 9396.
30 R. Nuñez, I. Romero, F. Teixidor and C. Viñas, *Chem. Soc. Rev.*, 2016, **45**, 5147.
31 I. Fuentes, M. J. Mostazo-López, Z. Kelemen, V. Compañ, A. Andrio, E. Morallón, D. Cazorla-Amorós, C. Viñas and F. Teixidor, *Chem.–Eur. J.*, 2019, **25**, 14308.
32 H. Djelad, F. Huerta, E. Morallón and F. Montilla, *Eur. Polym. J.*, 2018, **105**, 323.
33 H. Zhang, J. Li, C. Gu, M. Yao, B. Yang, P. Lu and Y. Ma, *J. Power Sources*, 2016, **332**, 413.
34 H. Zhou and X. Zhi, *Mater. Lett.*, 2018, **221**, 309.
35 H. W. Bode, *Network Analysis and Feedback Amplifier Design*, Van Nostrand, Princeton, NJ, USA, 1945.
36 D. Valverde, A. García-Bernabé, A. Andrio, E. García-Verdugo, S. V. Luis and V. Compañ, *Phys. Chem. Chem. Phys.*, 2019, **21**, 17923.
37 B. Altava, V. Compañ, A. Andrio, L. F. del Castillo, S. Mollá, M. I. Burguete, E. García-Verdugo and S. V. Luis, *Polymer*, 2015, **71**, 69.
38 H. Weingartner, *Angew. Chem., Int. Ed.*, 2008, **47**, 654.
39 T. E. Springer, T. Zawodzinski and S. Gottesfel, *J. Electrochem. Soc.*, 1991, **138**, 2334.
40 J. Otomo, N. Minagawa, C. Wen, K. Eguchi and H. Takahashi, *Solid State Ionics*, 2003, **156**, 357.
41 J. R. Lakowicz and G. Weber, *Biochemistry*, 1973, **12**, 4161.
42 M. Arık, N. Çelebi and Y. Onganer, *J. Photochem. Photobiol., A*, 2005, **173**, 105.
43 C. L. C. McCrory, S. Jung, I. M. Ferrer, S. M. Chatman, J. C. Peters and T. F. Jaramillo, *J. Am. Chem. Soc.*, 2015, **137**, 4347.
44 F. Teixidor, G. Barberà, A. Vaca, R. Kivekäs, R. Sillanpää, J. Oliva and C. Viñas, *J. Am. Chem. Soc.*, 2005, **127**, 10158.
45 S. Paavola, F. Teixidor, C. Viñas and R. Kivekäs, *J. Organomet. Chem.*, 2002, **657**, 187.
46 I. Guerrero, Z. Kelemen, C. Vinas, I. Romero and F. Teixidor, *Chem.–Eur. J.*, 2020, **26**, 5027.
47 P. Hosseinzadeh and Y. Lu, *Biochim. Biophys. Acta*, 2016, **1857**, 557.
48 R. Ashizawaa and T. Noguchi, *Phys. Chem. Chem. Phys.*, 2014, **16**, 11864.
49 M. Chaplin, *Nat. Rev. Mol. Cell Biol.*, 2006, **7**, 861.
50 R. Ruiz-Rosas, I. Fuentes, C. Viñas, F. Teixidor, E. Morallón and D. Cazorla-Amorós, *Sustainable Energy Fuels*, 2018, **2**, 345.
51 L. Mátel, F. Macášek, P. Rajec, S. Heřmánek and J. Plešek, *Polyhedron*, 1982, **1**, 511.
52 M. D. Mortimer, C. B. Knobler and M. F. Hawthorne, *Inorg. Chem.*, 1996, **35**, 5750.
53 P. K. Hurlburt, R. L. Miller, K. D. Abney, T. M. Foreman, R. J. Butcher and S. A. Kinkhead, *Inorg. Chem.*, 1995, **34**, 5215.
54 A. Andrio, S. I. Hernández, C. García-Alcántara, L. F. Del Castillo, V. Compañ and I. Santamaría-Holek, *Phys. Chem. Chem. Phys.*, 2019, **21**, 12948.
55 I. Fuentes, A. Andrio, F. Teixidor, C. Viñas and V. Compañ, *Phys. Chem. Chem. Phys.*, 2017, **19**, 15177.

